applied sciences

MDPI

Article

Measurement of Waveplate Parameters over Entire Clear Aperture Based on Differential Frequency Modulation with Dual Photoelastic Modulators

Kewu Li [1,2], Shuang Wang [2,3,*] and Zhibin Wang [2,*]

[1] School of Electrical and Control Engineering, North University of China, Taiyuan 030051, China; kewuli@nuc.edu.cn
[2] Engineering and Technology Research Center of Shanxi Province for Opto-Electric Information and Instrument, North University of China, Taiyuan 030051, China
[3] School of Data Science and Technology, North University of China, Taiyuan 030051, China
* Correspondence: 20200150@nuc.edu.cn (S.W.); wangzhibin@nuc.edu.cn (Z.W.)

Abstract: To obtain highly sensitive, accurate, fast, and repeatable measurements of waveplate parameters over an entire clear aperture, a novel measurement method using dual differential frequency photoelastic modulations is proposed. Simple polarimetry is conducted based on two photoelastic modulators, which operate at different frequencies. The fast-axis azimuth and retardance parameters of the waveplate are loaded into the modulation signals. Employing digital phase-locked technology, the fundamental and differential frequency harmonic terms are extracted, and then the two parameters of the waveplate are demodulated. The principle is analyzed, and the measurement system is built for verification experiments. The experimental results reveal that the two parameters of the waveplate are simultaneously measured over the entire clear aperture. The standard deviations of the fast-axis azimuth and retardance are 0.02° and 0.03 nm, respectively, and the maximum relative deviations of the fast-axis azimuth and retardance are 0.6% and 0.06%, respectively. The single-point data measurement time is only 200 ms. The proposed method exhibits high precision and speed, and provides an effective quality inspection and calibration method for waveplates.

Keywords: waveplate; photoelastic modulation; differential frequency modulation; fast-axis azimuth; retardance

check for updates

Citation: Li, K.; Wang, S.; Wang, Z. Measurement of Waveplate Parameters over Entire Clear Aperture Based on Differential Frequency Modulation with Dual Photoelastic Modulators. *Appl. Sci.* **2023**, *13*, 4496. https://doi.org/10.3390/app13074496

Academic Editor: Marilou Cadatal Raduban

Received: 21 March 2023
Revised: 28 March 2023
Accepted: 31 March 2023
Published: 1 April 2023

Copyright: © 2023 by the authors. Licensee MDPI, Basel, Switzerland. This article is an open access article distributed under the terms and conditions of the Creative Commons Attribution (CC BY) license (https://creativecommons.org/licenses/by/4.0/).

1. Introduction

A waveplate is a basic optical component manufactured based on birefringence [1]. It is typically made of quartz crystal, calcite crystal, MgF_2 crystal, or polymers with a thickness of tens of microns. The incident light is decomposed into ordinary and extraordinary light, with vibration directions perpendicular to each other. The ordinary light travels with the same velocity in every direction through the waveplate, and the extraordinary light travels with a velocity that is dependent upon the propagation direction within the waveplate. The main axis of the ordinary light refractive index is usually defined as the fast axis. After the two polarized light components pass through the waveplate, phase retardance is introduced. A waveplate is used to change the polarization state. Waveplates typically include a 1/4 waveplate, and a 1/2 waveplate, and the phase retardance corresponds to 90° and 180°, respectively. They are mainly employed in polarization-generating devices and polarization-analysis devices. It plays an important role in the fields of communication, sensing and optical storage [2–5]. The fast-axis azimuth and retardance are the key parameters of the waveplate. Accurate measurement and calibration of the two parameters over the entire aperture are key steps in the manufacturing process of the waveplate. These steps directly determine the performance of the polarization optical system using the waveplate.

Many waveplate parameter measurement studies have been conducted, including light intensity, polarization compensation, interferometry, laser feedback, and polarization

modulation techniques. In the light intensity method, the waveplate is placed between two orthogonal polarizers, the light intensity is obtained at different angles by rotating the waveplate, and the retardance of the waveplate is calculated [6]. The polarization compensation method is based on the Sénarmont compensation principle [7]. In accordance with the light intensity method, a compensator with a known retardance is added between the waveplate and the analyzer. Waveplate measurement is realized by observing the polarization angle produced by rotating the compensator or analyzer. Light intensity and polarization compensation methods have the advantages of a simple instrument structure and low cost. However, these two methods require the mechanical rotation of the sample and multiple measurements at different angles to measure the waveplate parameters. The measurement accuracy is limited, and the requisite multiple measurements are time-consuming, making them unsuitable for rapid measurement. Michelson interferometry or Mach–Zehnder interferometry is used to insert the waveplate into the measurement optical path [8]. The retardance of the waveplate can be calculated according to the optical path difference between the measurement and reference optical paths. This method has high measurement accuracy. Nevertheless, it is easily disturbed by environmental factors, such as temperature and environmental vibrations. Meanwhile, the laser feedback method incorporates the waveplate to be tested in the laser feedback cavity [9]. The length of the feedback cavity is scanned by a piezoelectric ceramic-driven mirror, and the polarization jump of the laser output light intensity is detected to realize the waveplate retardance measurement. The sample needs to be coated with a narrowband filter film for single-laser mode wavelengths. The measurement accuracy depends on the light intensity stability, and the measurement accuracy and repeatability are affected by the ambient temperature and vibration.

Polarization modulation methods, such as electro-optic modulation, magneto-optical modulation, and photoelastic modulation, are used to measure the waveplate parameters [10]. Polarization modulation methods realize the modulation of light intensity, and alternating current (AC) light intensity signals are achieved. The waveplate parameters are loaded into the AC signals, and the measurements are completed by utilizing the change in the AC signal amplitude. The signal-to-noise ratio is thereby improved, and a more precise measurement is achieved. Compared with Faraday rotators and electro-optic modulators, the photoelastic modulator (PEM) has application advantages, such as a high modulation frequency, a large optical aperture, high modulation purity, and stable operation [11]. Zeng et al. developed a waveplate measurement system based on photoelastic modulation [12]. A single PEM is used, and the direct current (DC), the first and second harmonic terms of the photoelastic modulation are measured to obtain the waveplate parameters. However, none of the current measurement methods can realize simultaneous measurement of the two parameters of the waveplate retardance and fast-axis azimuth in a single measurement. Accurate measurement and calibration of the waveplate over the entire clear aperture are critical for the application of polarization optical systems with a large field of view and a large clear aperture.

In this study, we developed a differential frequency modulation approach that leverages the advantages of the PEM. It employs dual PEMs, and digital phase-locked data processing technology is used to demodulate the signals. Moreover, a high-speed, high-precision waveplate parameters measurement method is demonstrated. The parameters over the entire clear aperture of the waveplate are measured by equipping it with a two-dimensional motorized scanning stage.

2. Principle

Leveraging the advantages of the high modulation frequency, large optical aperture, and high modulation purity of photoelastic modulation, and combining them with digital phase-locked data processing technology, a measurement method for waveplate parameters is developed. It is based on differential frequency modulation using dual PEMs. Simultaneous measurements of the waveplate phase retardance and fast-axis azimuth

are carried out, and the distribution measurements of the parameters on the aperture are performed by scanning the sample in an electric translation stage. The basic principles of the measurement scheme are illustrated in Figure 1.

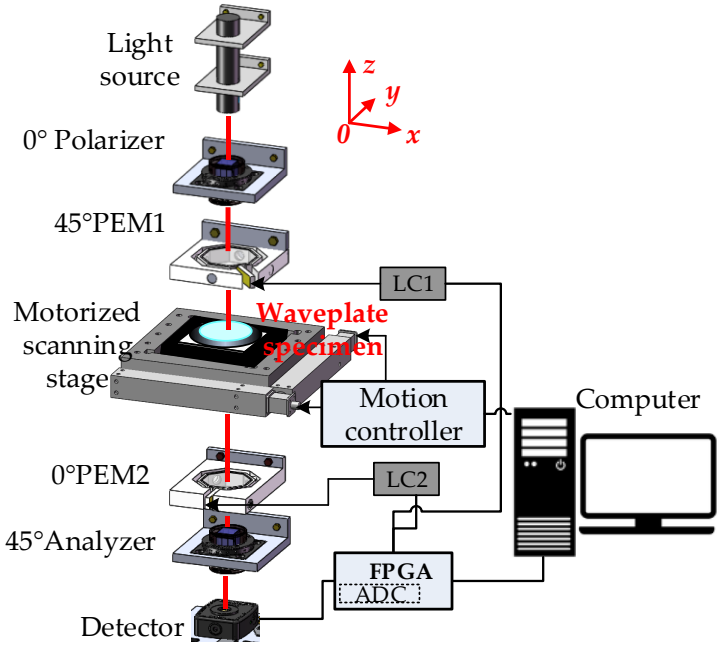


Figure 1. Schematic diagram of waveplate parameter measurement. FPGA: field programmable gate array; LC: inductance–capacitance resonant driving circuit; ADC: analog-to-digital converter.

As shown in Figure 1, a polarization analysis system is built using PEM1 and PEM2 as the core. The detection laser passes through the polarizer and the two PEMs in turn. It then passes through the analyzer that will be identified by the detector. The transmission axis directions of the polarizer and analyzer are set to 0° and 45°, respectively, and the modulation fast-axis directions of the two PEMs are set to 45° and 0°, respectively. Throughout the polarization analysis device, the direction of the transmission axis of the polarizer and the direction of the fast axis of the PEMs are sequentially different by 45°.

To realize the simultaneous measurement of the phase retardance and fast-axis azimuth, the two PEMs are designed to have different resonant operating frequencies. They operate in cascade, which forms a differential frequency modulation polarization analysis and measurement system. The sample is placed between the PEMs, and a motorized scanning table is used. The optical signal detection is described by the Stokes vector, and the polarization transmission characteristics of the polarizer, PEM, and sample are described by the Muller matrix [13]. The entire measurement scheme is described by the Stokes vector and Muller matrix as

$$S_{out} = M_A M_{PEM2} M_S M_{PEM1} S_{in} \quad (1)$$

wherein S_{out} represents the Stokes vector of outgoing light, and S_{in} denotes the Stokes vector of incident light after passing through the 0° polarizer. It is usually expressed as $S_{in} = I_0[1 \quad 1 \quad 0 \quad 0]^T$, where I_0 is the total intensity of the incident light transmitted through the polarizer. M_{PEM1} and M_{PEM2} represent the Muller matrices of PEM1 and PEM2, respectively. The modulation fast-axis azimuth of PEM1 is set at 45°, and the modulation fast-axis azimuth of PEM2 is set at 0°. Accordingly, the Muller matrices of the two PEMs can be described as follows [11].

$$M_{PEM1} = \begin{bmatrix} 1 & 0 & 0 & 0 \\ 0 & \cos\delta_1 & 0 & \sin\delta_1 \\ 0 & 0 & 0 & 0 \\ 0 & -\sin\delta_1 & 0 & \cos\delta_1 \end{bmatrix} \text{ and } M_{PEM2} = \begin{bmatrix} 1 & 0 & 0 & 0 \\ 0 & 1 & 0 & 0 \\ 0 & 0 & \cos\delta_2 & -\sin\delta_2 \\ 0 & 0 & \sin\delta_2 & \cos\delta_2 \end{bmatrix}, \quad (2)$$

where δ_1 and δ_2 represent the modulation phases of PEM1 and PEM2. The modulation phase can be further expressed as $\delta_1 = \delta_{10} \sin \omega_1 t$ and $\delta_2 = \delta_{20} \sin \omega_2 t$, where δ_{10} and δ_{20} represent the phase modulation amplitudes of the two PEMs, and ω_1 and ω_2 represent the resonant operating frequencies of the two PEMs, respectively. To realize the simultaneous measurement of the waveplate phase retardance and fast-axis azimuth angle, the key to our proposed scheme is that the resonant operating frequencies of the two PEMs are not equal ($\omega_1 \neq \omega_2$), which engenders the polarization analysis measurement system with dual PEM cascaded differential frequency modulation.

The polarization transfer characteristics of the waveplate can be described by the Muller matrix (M_S) as follows [1,12].

$$M_S = \begin{bmatrix} 1 & 0 & 0 & 0 \\ 0 & \cos^2(2\theta) + \sin^2(2\theta) \cdot \cos(\phi) & \sin(4\theta) \cdot \sin^2(\phi/2) & \sin(2\theta)\sin(\phi) \\ 0 & \sin(4\theta) \cdot \sin^2(\phi/2) & \sin^2(2\theta) + \cos^2(2\theta) \cdot \cos(\phi) & -\cos(2\theta)\sin(\phi) \\ 0 & -\sin(2\theta)\sin(\phi) & \cos(2\theta)\sin(\phi) & \cos(\phi) \end{bmatrix} \quad (3)$$

where ϕ is the phase retardance. It can be further expressed as $\phi = \frac{2\pi}{\lambda}(n_e - n_o)d$, where λ is the wavelength of incident light, d is the thickness of the waveplate, and n_o and n_e are the refractive indices of ordinary and extraordinary light, respectively. θ is the fast-axis azimuth. It can be observed from the above formula that the polarization characteristics of the waveplate are fully determined by the two parameters of phase retardance ϕ and fast-axis azimuth θ. They must be strictly measured and calibrated, especially the parameters over the entire clear aperture.

Furthermore, the transmission axis of the analyzer is set at 45°, and its Muller matrix (M_A) is expressed as follows.

$$M_A = \frac{1}{2}\begin{bmatrix} 1 & 0 & 1 & 0 \\ 0 & 0 & 0 & 0 \\ 1 & 0 & 1 & 0 \\ 0 & 0 & 0 & 0 \end{bmatrix} \quad (4)$$

Here, we insert into Equation (1) the Muller matrices of the PEMs, waveplate, and analyzer expressed in Equations (2)–(4), together with the Stokes vector of incident light. We consider that the light intensity perceived by the detector is the first component of the Stokes vector [13,14]. It can, thus, be solved to obtain the output light intensity detected by the detector to the measurement system as follows.

$$\begin{aligned} I = \tfrac{I_0}{2}(1 + \cos\delta_1 \cos\delta_2 \sin(4\theta) \sin^2(\tfrac{\phi}{2}) + \sin\delta_1 \sin\delta_2 \cos\phi + \\ + \cos\delta_1 \sin\delta_2 \cos(2\theta) \sin\phi + \sin\delta_1 \cos\delta_2 \sin(2\theta) \sin\phi) \end{aligned} \quad (5)$$

In the formula above, the two PEM modulation items, $\sin\delta_i = \sin(\delta_{i0} \sin\omega_i t)$ and $\cos\delta_i = \cos(\delta_{i0} \sin\omega_i t)$, are expanded as $\sin\delta_i = 2\sum_{2k-1} J_{2k-1}(\delta_{i0}) \sin((2k-1)\omega_i t)$ and $\cos\delta_i = J_0(\delta_{i0}) + \sum_{2k} 2J_{2k}(\delta_{i0}) \cos(2k\omega_i t)$ using the first kind of Bessel functions; $k = 1, 2, \cdots$ are positive integers; J_0, J_{2k-1}, and J_{2k} represent the Bessel series of the 0th order, the $(2k-1)$th order, and the $2k$th order, respectively [11,15,16]. Additionally, PEM1 and PEM2 correspond to i = 1 and 2, respectively. Taking k = 1 as the low-order Bessel series, Equation (5) can be further rewritten as follows.

$$\begin{aligned} I = \tfrac{I_0}{2}(1 + (J_0(\delta_{10}) + 2J_2(\delta_{10})\cos(2\omega_1 t)) \cdot (J_0(\delta_{20}) + 2J_2(\delta_{20}) \cdot \cos(2\omega_2 t)) \sin(4\theta) \sin^2(\tfrac{\phi}{2}) \\ + 4J_1(\delta_{10}) J_1(\delta_{20}) \sin(\omega_1 t) \sin(\omega_2 t) \cos\phi + (J_0(\delta_{10}) + 2J_2(\delta_{10}) \cos(2\omega_1 t)) \cdot (2J_1(\delta_{20}) \sin(\omega_2 t)) \cdot \\ \cos(2\theta) \sin\phi + (J_0(\delta_{20}) + 2J_2(\delta_{20}) \cos(2\omega_2 t)) \cdot (2J_1(\delta_{10}) \sin(\omega_1 t)) \sin(2\theta) \sin\phi) \end{aligned} \quad (6)$$

From the analysis of Equation (6), it can be observed that the relevant terms for the waveplate phase retardance and fast-axis azimuth are loaded in different frequency signals. The relevant term $\sin(4\theta)\sin^2(\phi/2)$ is loaded into $2\omega_1$, $2\omega_2$, $2\omega_1 + 2\omega_2$, and $2\omega_2 - 2\omega_1$

signals, and the relevant term $\cos\phi$ is loaded into $\omega_2 - \omega_1$ and $\omega_1 + \omega_2$ signals. The relevant term $\cos(2\theta)\sin\phi$ is loaded into ω_2, $2\omega_1 + \omega_2$ and $2\omega_1 - \omega_2$ signals, and the relevant term $\sin(2\theta)\sin\phi$ is loaded into ω_1, $2\omega_2 + \omega_1$ and $2\omega_2 - \omega_1$ signals. By solving the differential frequency signal components of dual photoelastic modulation, simultaneous measurement of the retardance and the fast-axis azimuth can be realized. Digital phase-locking technology is used to control the analog-to-digital (AD) sampling frequency through the field programmable gate array (FPGA), and the digital signal sequence of the detected light intensity after AD conversion is input into the FPGA [11,15,16]. The fundamental frequency harmonic terms of the two PEMs, V_{ω_1} and V_{ω_2}, and the different frequency harmonic terms, $V_{\omega_2-\omega_1}$, are simultaneously demodulated.

$$\begin{cases} V_{\omega 1} = I_0 J_0(\delta_{20}) J_1(\delta_{20}) \sin(2\theta)\sin\phi \\ V_{\omega 2} = I_0 J_0(\delta_{10}) J_1(\delta_{20}) \cos(2\theta)\sin\phi \\ V_{\omega 2-\omega 1} = I_0 J_1(\delta_{10}) J_1(\delta_{20}) \cos\phi \end{cases} \tag{7}$$

For the convenience of data calculation, the ratio of the fundamental frequency signal (V_{ω_1}, V_{ω_2}) to the differential frequency signal ($V_{\omega_2-\omega_1}$) of the two PEMs is calculated, and the ratios of the two channels are defined as R_{I} and R_{II}.

$$\begin{cases} R_{\mathrm{I}} = \frac{V_{\omega 1} J_1(\delta_{20})}{V_{\omega 2-\omega 1} J_0(\delta_{20})} = \sin(2\theta)\tan\phi \\ R_{\mathrm{II}} = \frac{V_{\omega 2} J_1(\delta_{10})}{V_{\omega 2-\omega 1} J_0(\delta_{10})} = \cos(2\theta)\tan\phi \end{cases} \tag{8}$$

Using the above ratio, phase retardance ϕ and fast-axis azimuth θ are simultaneously solved.

$$\begin{cases} \theta = \frac{1}{2}\arctan\left(\frac{R_{\mathrm{I}}}{R_{\mathrm{II}}}\right) \\ \phi = \arctan\left(\sqrt{{R_{\mathrm{I}}}^2 + {R_{\mathrm{II}}}^2}\right) \end{cases} \tag{9}$$

The phase retardance of the waveplate is usually expressed by the retardance, and $\Phi = \phi\lambda/2\pi$. The scheme in this study can simultaneously measure the waveplate parameters through a single measurement of the polarization analysis system with dual cascade differential frequency photoelastic modulation. Combined with a motorized scanning stage to push the waveplate, parameter distribution measurements on the entire aperture of the waveplate are performed.

3. Experiment

The experimental system was built as shown in Figure 1. The detection light source is a NewOpto-633-2-P helium-neon laser from Hangzhou New Power Optoelectronics Technology Co., Ltd. (HangZhou, Zhejiang, China), with a wavelength of 632.8 nm, an optical power of 2 mW, and a spot size of 2 mm. The polarizer and analyzer are Glan–Taylor polarizers, and the extinction ratio is up to 10^5:1. PEM1 and PEM2 are both single-drive octagonal symmetrical PEMs developed by us, the piezoelectric driver is piezoelectric quartz crystal, and the optical crystal is fused quartz crystal. The length, width and thickness of the fused silica crystal of PEM1 and PEM2 are 60 mm × 60 mm × 16 mm and 54.2 mm × 54.2 mm × 16 mm, respectively. The resonant frequencies of the two PEMs are 44.912 kHz and 49.953 kHz, respectively. The motorized scanning stage is a precision two-dimensional electric translation stage (EPSD150-150, Wuhan Hongxingyang Technology Co., Ltd., Wuhan, China) with an XY stroke of 150 × 150 mm, a maximum scanning speed of 6 mm/s, and a positioning accuracy of 50 μm.

The motorized scanning stage is equipped with a clamping fixture whose size could be flexibly adjusted according to the sample size. The used detector is a silicon photodetector (DH-GDT-D020V, Beijing Daheng New Era Technology Co., Ltd., Beijing, China). The PEM driving and data processing circuit is manufactured using an Altera EPC IV FPGA chip as the core. The two PEM driving signal sources used the DDS module of the FPGA to provide driving square wave signals, which are amplified by the LC resonant circuit to

drive the PEMs. The modulated light intensity signal is detected using a photodetector. Signal acquisition is implemented using a 12-bit high-precision analog-to-digital converter (ADC), and the digital signal sequences are input into the FPGA digital phase-locked data processing module [15,16]. The data processing of the harmonic terms of V_{ω_1}, V_{ω_2}, and $V_{\omega_2-\omega_1}$ is then simultaneously completed.

3.1. Phase Modulation Amplitude Setting and System Initial Offset Calibration

PEM is an optical electromechanical device with resonant characteristics. The phase modulation amplitude of the processed PEM is proportional to the peak-to-peak value of the driving voltage, and the phase modulation amplitude can be precisely adjusted by the driving voltage [11]. From the theoretical analysis of Equations (5)–(7), it is necessary to reasonably set the phase modulation amplitudes of the two PEMs, which makes the 0th and 1st order Bessel series, J_0 and J_1, take the maximum value, and the amplitudes of the fundamental frequency harmonic terms (V_{ω_1} and V_{ω_2}) and the difference frequency harmonic term ($V_{\omega_2-\omega_1}$) are large. Thus, the fundamental frequency and difference frequency signals are the main components of the modulated light intensity signals, and a high signal-to-noise ratio for data processing is obtained. The numerical calculations of the Bessel series that varies with the PEM phase modulation amplitude are shown in Figure 2.

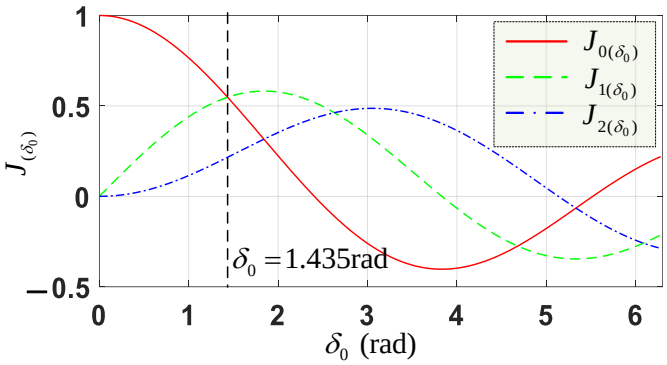


Figure 2. Bessel series variation in accordance with PEM phase modulation amplitude.

As shown in Figure 2, when the phase modulation amplitudes of the two PEMs are set near 1.435 rad, the Bessel series terms, J_0J_1 and J_1J_1, take the maximum value. In this study, the peak-to-peak driving voltages of the two PEMs are set to 190.5 V and 189.2 V, respectively, so that the phase modulation amplitude reaches 1.435 rad.

First, when no sample is used, the detection light signal is modulated by the two PEMs and the modulated light intensity signals are digitally phase-locked for data processing to complete the calibration of the initial value of the system. The digital phase-locking cycle is set to 1008 cycles for the differential frequency signal, i.e., $\omega_2 - \omega_1$ = 5.041 kHz, and the data point is measured at an interval of 200 ms. The fundamental harmonic terms (V_{ω_1} and V_{ω_2}) and the difference frequency harmonic terms ($V_{\omega_2-\omega_1}$) are extracted and recorded, as shown in Figure 3.

When no sample is used, the differential frequency harmonic term ($\overline{V}_{\omega_2-\omega_1} = 3.899 \times 10^8$ a.u.) is much larger than the two fundamental harmonic terms ($\overline{V}_{\omega_1} = 2.077 \times 10^5$ a.u. and $\overline{V}_{\omega_2} = 6.254 \times 10^5$ a.u.), and the harmonic term ratios are small, ($\overline{R}_{\mathrm{I}} = 0.533 \times 10^{-3}$ and $\overline{R}_{\mathrm{II}} = 1.604 \times 10^{-3}$). In fact, when there is no sample, the two ratios should approach zero. This is mainly due to the small residual birefringence of the two PEMs. However, the two PEMs in the system are elaborately manufactured, and the harmonic term ratios do not exceed the order of 10^{-3}. To achieve high-precision measurement of the waveplate parameters, this study regards the above two non-zero ratios as the initial offset values of the system. In actual measurements, the obtained signal ratio must be subtracted from the initial offset value of the system to reduce or eliminate the system measurement error to the greatest extent possible.

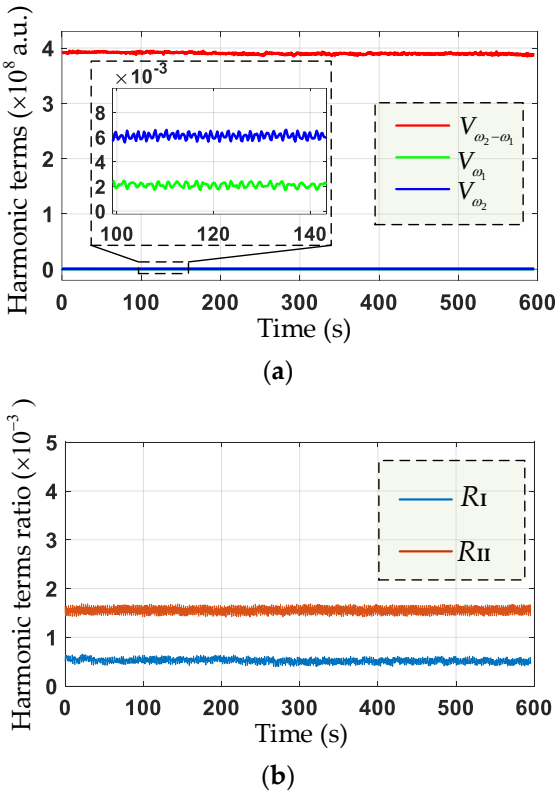


Figure 3. Digital phase-lock result of modulation signals: (**a**) amplitude of harmonic terms; (**b**) ratio of harmonic terms.

3.2. Waveplate Parameter Measurement Experiment

The measurement accuracy and repeatability of the proposed scheme are determined. First, we select a 1/4 waveplate sample at the wavelength of 632.8 nm for the experiment. During the experiment, the temperature of the laboratory is set at 23 °C, and the temperature fluctuation does not exceed 0.1 °C during the entire experiment. The 1/4 waveplate is a compound zero-order waveplate (GCL-060402), produced by Beijing Daheng New Era Technology Co., Ltd. The accuracy of the waveplate retardance is λ/300. The size of the waveplate is 1 inch. It is installed on a rotatable mirror frame with an angular rotation accuracy of 5′. The effective clear aperture is 22 mm after the optical kit holding. The waveplate is placed in the middle of the scanning stage. The detection laser light passes through the center of the waveplate, and the azimuth angle of the fast axis of the waveplate is adjusted to 22.5°. The harmonic terms obtained by digital phase-locking are shown in Figure 4.

In Figure 4a, the differential frequency harmonic terms are almost zero, and the values of the two fundamental frequency harmonic terms are very close. The harmonic terms (V_{ω_1}, V_{ω_2}, and $V_{\omega_2-\omega_1}$) and Bessel series are substituted into Equations (7) and (8). Accordingly, the two parameters of the waveplate retardance and fast-axis azimuth can be further solved, as shown in Figure 4b. The test record lasts for approximately 1 min, with approximately 200 test data points. The measurement results show that the average fast-axis azimuth of the waveplate is $\overline{\theta} = 22.49°$, the standard deviation is $\sigma_\theta = 0.02°$, and the average retardance of the waveplate is $\overline{\Phi} = 158.43$ nm, and the standard deviation is $\sigma_\Phi = 0.03$ nm, indicating that the measurement system in this study has good stability and repeatability. Parameter measurements are also performed at different azimuth angles. The fast-axis azimuth of the waveplate is adjusted from 0° to 180° at intervals of 20°, and the results are recorded in Figure 5.

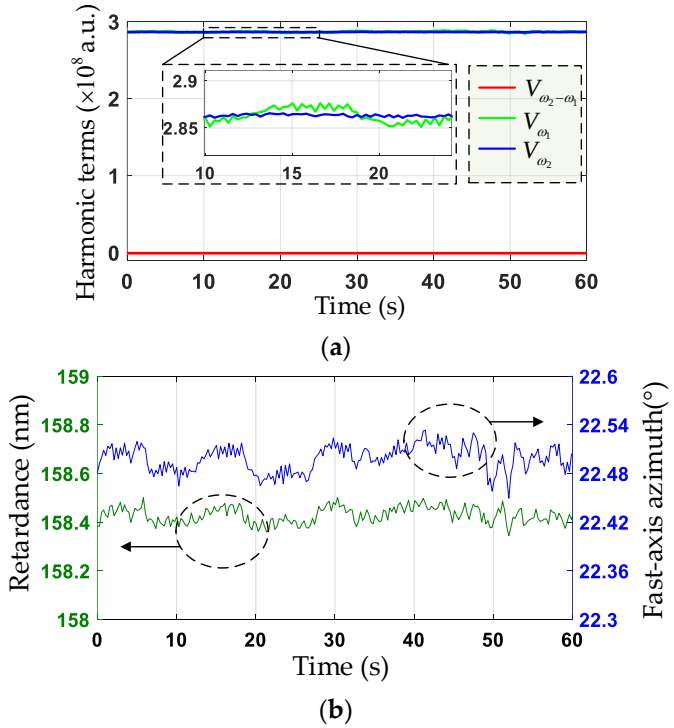


Figure 4. The 1/4 waveplate parameter experimental results: (**a**) harmonic terms; (**b**) waveplate parameter measurement values.

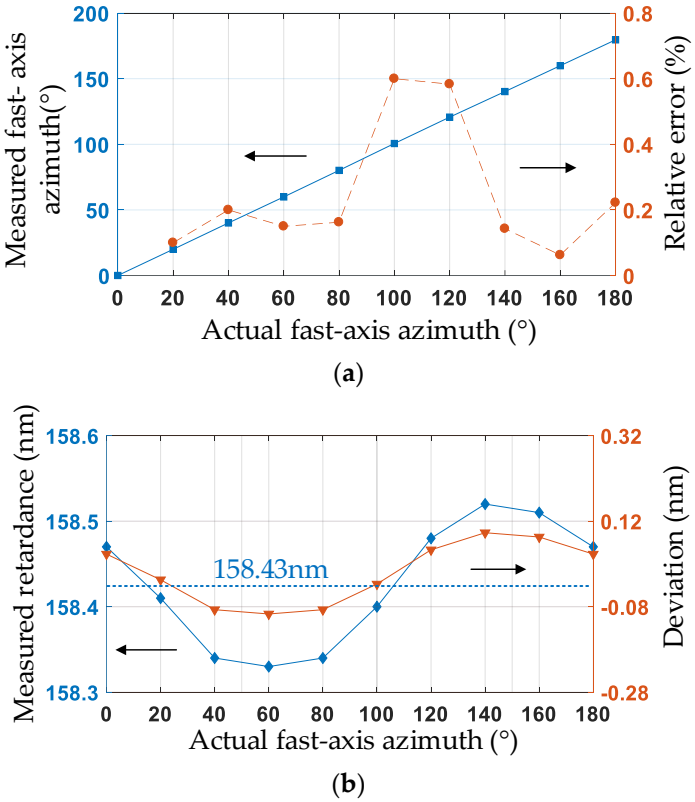


Figure 5. The 1/4 waveplate parameter experimental results under different angles: (**a**) fast-axis azimuth; (**b**) retardance at different fast-axis azimuths.

In Figure 5a, the fast-axis azimuth angle measurements and actual values are in good agreement. When the fast-axis azimuth is rotated at 100°, the measured value is

100.6°, and there is a maximum relative deviation, i.e., $\frac{\Delta_\theta}{\theta} = \frac{100.6-100}{100} \times 100\% = 0.6\%$. In Figure 5b, the deviation between the retardance measurement and actual value is notably small. When the fast-axis azimuth is rotated at the position of 60°, the measured value of the waveplate retardance is 158.33 nm, there is a maximum deviation of $\Delta_\Phi = \left|\Phi - \overline{\Phi}\right| = |158.33 - 158.43| = 0.1$ nm, and the corresponding maximum relative deviation is $\frac{\Delta_\Phi}{\Phi} = \frac{0.1}{158.43} \times 100\% = 0.06\%$. The results show that the system realizes the measurement of the waveplate parameters with high precision.

3.3. Waveplate Parameter Measurement in the Entire Aperture

To further realize the parameter measurements in the entire aperture, the fast-axis azimuth of the waveplate is rotated to an initial angle, and the precise two-dimensional electric translation stage is initiated to scan the 26 × 26 mm area at 2 mm intervals. The waveplate parameters in the entire clear aperture are shown in Figure 6. The entire measurement area requires 1 min. For the visual display, the retardance at each spatial position is represented by a color chart, and the fast-axis azimuth is directly drawn as a straight line at each image position over the scanning zone.

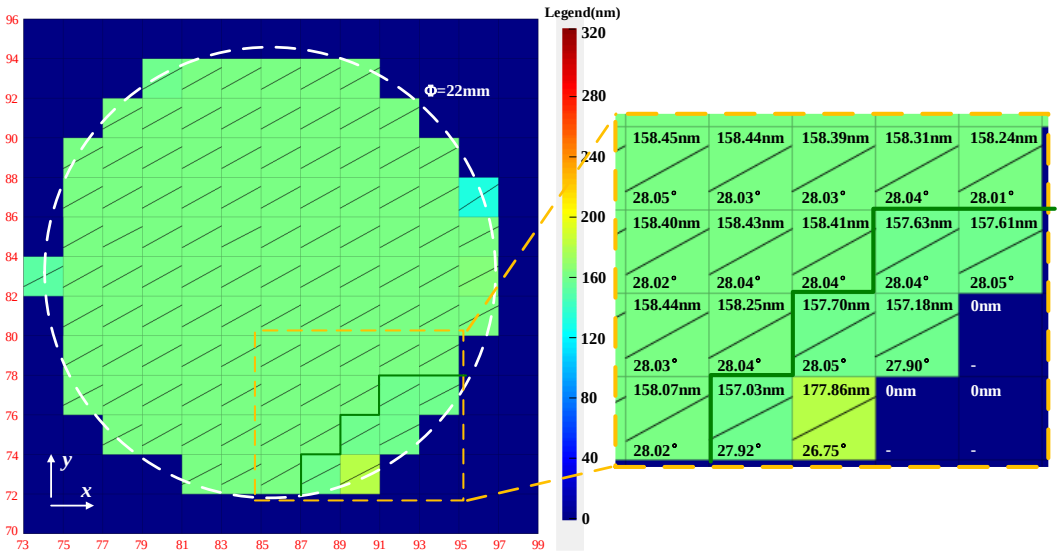


Figure 6. The 1/4 waveplate parameters measurements results for the entire aperture.

The results in Figure 6 show that the retardance and fast-axis azimuth parameters of the 632.8 nm 1/4 waveplate are consistent for the entire clear aperture, and the retardance values are generally distributed around 160 nm. However, outlier data points are observed at the edges of the scanned area. In the lower right area of the waveplate, the retardance values are slightly smaller. The area is subsequently further enlarged, as shown in Figure 6. The measurements of the two parameters in the entire light-passing area of the waveplate are recorded, as shown in Table 1.

Table 1. The 1/4 waveplate parameter measurements for the entire aperture.

Retardance (nm)	Legend	Data Points	Fast-Axis Azimuth
131.49		1	33.6
149.03		1	27.85
157.4 ± 0.5		5	27.99 ± 0.07
158.4 ± 0.5		94	28.03 ± 0.02
175.5 ± 0.5		1	26.75

It can be observed from the measurement data that the retardance of the entire clear aperture of the waveplate is mainly distributed in the range of (158.4 ± 0.5) nm. There

are 94 data points, accounting for 92% of the total 102 data points. Three data outliers are observed at the edge of the waveplate. In the lower right area, there is a small section where the waveplate retardance is 1 nm smaller than the average value; however, it still meets the manufacturing retardance accuracy of λ/300 (approximately 2.1 nm@λ = 632.8 nm). Except for the data outliers, the fast-axis azimuth of the waveplate is about 28°. The 1/4 and 1/2 waveplates at the wavelength of 532 nm, namely GCL-060401 and GCL-060411 (Beijing Daheng New Era Technology Co., Ltd.), are also measured. The results for the full clear apertures of the two waveplates are shown in Figure 7.

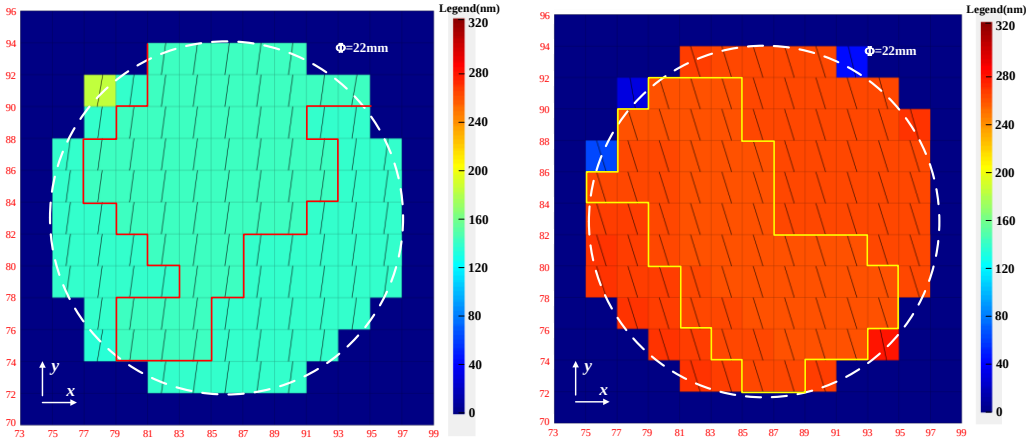


Figure 7. Waveplate parameter measurement results of the 532 nm waveplate in the entire clear aperture: (**a**) 1/4 waveplate; (**b**) 1/2 waveplate.

In Figure 7, it can be observed that the retardance values of the 1/4 and 1/2 waveplates are mainly distributed in two value ranges; however, the difference is small, and the fast-axis azimuth for the entire waveplate aperture is generally consistent; the retardance value of the 1/4 waveplate is approximately 130 nm, and that of the 1/2 waveplate is approximately 270 nm. The measurement results depicted in Figure 7 are outlined in Table 2.

Table 2. The 532 nm waveplate parameter measurements.

Waveplate	Retardance (nm)	Legend	Data Points	Fast-Axis Azimuth
1/4 Waveplate	135.0 ± 0.5		48	83.33 ± 0.03
	136.5 ± 0.5		53	83.33 ± 0.03
	179.28		1	82.53
1/2 Waveplate	61 ± 0.5		3	109.10 ± 0.4
	265.6 ± 0.5		36	109.40 ± 0.03
	268 ± 1		63	109.40 ± 0.03

From the statistical results, except for the numerical anomalies, the retardance value of the 1/4 waveplate is almost completely distributed between 134.5 nm and 137 nm. The fast-axis azimuth is around 83.33°. Furthermore, the 1/2 waveplate retardance is generally distributed between 265.1 nm and 269 nm. The fast-axis azimuth is around 109.40°. In this study, the proposed system realizes the measurement of the retardance and the fast-axis azimuth in the whole aperture range of the waveplate.

4. Discussion

Based on dual differential frequency photoelastic modulation, the simultaneous measurement of the two parameters of waveplate retardance and fast-axis azimuth is realized. The measurement results of the 1/4 waveplate show that the standard deviation of the

fast-axis azimuth is $\sigma_\theta = 0.02^\circ$, and the measurement standard deviation of the retardance is $\sigma_\phi = 0.03$ nm. These findings demonstrate that the proposed measurement system has good stability and repeatability. Highly sensitive waveplate parameters measurements are realized. The maximum relative deviation of the fast-axis azimuth measurement obtained by rotating the entire waveplate is 0.6%, and the maximum relative deviation of the waveplate retardance measurement is 0.06%, indicating that the test system in this study achieves high-precision waveplate parameter measurements. In addition, the system data processing is based on FPGA digital phase-locking technology, which can simultaneously eliminate measurement influences such as the fluctuation in laser light intensity. The single-point data measurement time is only 200 ms, which is suitable for fast measurements. Moreover, the presented method is compatible with the two-dimensional motorized scanning stage, which can support parameter measurements in the entire waveplate light transmission range, and the maximum area can be 150 × 150 mm in this system. The test results of this study are compared with those in the existing literature, and are listed in Table 3.

Table 3. Comparison with reported waveplate measurement methods.

Method	Standard Deviation of Fast-Axis Azimuth σ_θ(°)	Standard Deviation of Retardance σ_ϕ (nm)	Simultaneous Measurements (Yes/No)	Measurement Time	Surface Distribution Measurement. (Yes/No)	Ref.
Sénarmont compensation method	0.1°	±5 nm	No	1 min	No	[7]
Interferometry	0.22°	0.37° (0.65 nm@632.8 nm)	Yes	1 s	No	[8]
Laser feedback		0.12° (0.21 nm@632.8 nm)	No	-	No	[9]
Single photoelastic modulation	0.5°	0.17° (0.30 nm@632.8)	Yes	-	No	[12]
Differential frequency modulation with dual photoelastic modulation	0.02°	0.03 nm	Yes	200 ms	Yes	Present work

The proposed method achieves higher repeatability, greater precision, and faster waveplate parameter measurements than the existing methods. Moreover, the presented scheme can simultaneously measure the parameters of the entire light-passing area of the waveplate. Through the test results of the entire light-passing area, it is evident that the retardance and fast axis of the waveplate in the entire light-passing area are clearly shown, providing a comprehensive understanding of waveplate parameters. Therefore, the proposed approach serves as an effective quality inspection and calibration method for waveplates. However, the individual abnormal data points at the edges of the waveplate parameters should be eliminated. It is estimated that the laser is blocked or reflected by the edge of the rotating mirror frame, causing measurement errors. This should be eliminated when testing the quality of the waveplate.

Moreover, it is worth noting that this study uses a He-Ne laser as the detection light source. The wavelength of the light source is 632.8 nm, and the spectral bandwidth is less than 2 pm, which can achieve the precise retardance of the waveplate at this wavelength. However, when it is applied to waveplates of other wavelengths, the spectral dispersion of the waveplate material should be considered to ensure accuracy. We will expand on and develop this topic in future work.

5. Conclusions

In summary, a measurement method for waveplate parameters based on differential frequency modulation with dual PEMs is presented. The principle of the method is established. A measurement system is built, and experiments are carried out. The measurement results reveal that the standard deviations of the fast-axis azimuth and retardance are 0.02° and 0.03 nm, respectively, and the maximum relative deviations of fast-axis azimuth and retardance is 0.6% and 0.06%, respectively. The two parameters of fast-axis azimuth and retardance are simultaneously measured, and the single-point data measurement time is only 200 ms. The proposed method cooperates with a two-dimensional motorized scanning

stage, which can realize the parameter measurements in the entire waveplate light transmission range, and the maximum area can be 150 × 150 mm in this system. The proposed method demonstrates high-precision, high-speed, highly stable and repeatable, and highly sensitive waveplate parameter measurements.

Author Contributions: Methodology, K.L. and S.W.; software, K.L.; formal analysis, K.L. and Z.W.; validation, K.L.; investigation, K.L. and Z.W.; resources, Z.W.; data curation, K.L.; writing—original draft preparation, K.L. and S.W.; writing—review and editing, K.L.; supervision, S.W. and Z.W. All authors have read and agreed to the published version of the manuscript.

Funding: This research was funded by the National Natural Science Foundation of China (62205309); the National Natural Science Foundation of China (62205310).

Institutional Review Board Statement: Not applicable.

Informed Consent Statement: Not applicable.

Data Availability Statement: Not applicable.

Conflicts of Interest: The authors declare no conflict of interest.

References

1. Kliger, D.S.; Lewis, J.W.; Randall, C.E. *Polarized Light in Optics and Spectroscopy*; Academic Press: Boston, MA, USA, 1990; pp. 39–52. [CrossRef]
2. Chen, K.-H.; Chu, Y.-C.; Chen, J.-H. Applying the phase difference property of polarization angle for measuring the concentration of solutions. *Opt. Laser Technol.* **2012**, *44*, 251–254. [CrossRef]
3. Mu, S.; Shi, Y.; Song, Y.; Liu, W.; Wei, W.; Gong, Q.; Dong, D.; Shi, K. Multislice computational model for birefringent scattering. *Optica* **2023**, *10*, 81–89. [CrossRef]
4. He, H.; Liao, R.; Zeng, N.; Li, P.; Chen, Z.; Liu, X.; Ma, H. Mueller Matrix Polarimetry—An Emerging New Tool for Characterizing the Microstructural Feature of Complex Biological Specimen. *J. Light. Technol.* **2019**, *37*, 2534–2548. [CrossRef]
5. Maria, S.; Bernardis, P.D.; Masi, S. Modeling Transmission and Reflection Mueller Matrices of Dielectric Half-Waveplates. *J. Infrared Millim. Terahertz Waves* **2017**, *38*, 215–228.
6. Wang, W.; Chen, J. Simple method for simultaneous determination of the phase retardation and fast axis of a waveplate. *Optik.* **2013**, *124*, 4359–4363. [CrossRef]
7. Montarou, C.C.; Gaylord, T.K. Two-wave-plate compensator method for single-point retardation measurements. *Appl. Opt.* **2004**, *43*, 6580–6595. [CrossRef] [PubMed]
8. Chen, K.; Lin, C.; Liu, P. An interferometric method for simultaneously determination the phase retardation and fast-axis azimuth angle of a waveplate. *J. Mod. Optic.* **2020**, *67*, 992–997. [CrossRef]
9. Chen, W.; Long, X.; Zhang, S.; Xiao, G. Phase retardation measurement by analyzing flipping points of polarization states in laser with an anisotropy feedback cavity. *Opt. Laser Technol.* **2012**, *44*, 2427–2431. [CrossRef]
10. Zhang, P.; Tan, Y.; Liu, W.; Chen, W. Methods for optical phase retardation measurement: A review. *Sci. China Technol. Sci.* **2013**, *56*, 1155–1164. [CrossRef]
11. Wang, S.; Han, X.; Wang, Y.; Li, K. Dispersion of the Retardation of a Photoelastic Modulator. *Appl. Sci.* **2019**, *9*, 341. [CrossRef]
12. Zeng, A.; Huang, L.; Dong, Z.; Hu, J.; Huang, H.; Wang, X. Calibration method for a photoelastic modulator with a peak retardation of less than a half-wavelength. *Appl. Opt.* **2007**, *46*, 699–703. [CrossRef] [PubMed]
13. Liu, Y.W.; Jones, G.A.; Peng, Y.; Shen, T.H. Generalized theory and application of Stokes parameter measurements made with a single photoelastic modulator. *J. Appl. Phys.* **2006**, *100*, 063537. [CrossRef]
14. Satozono, H. Elimination of artifacts derived from the residual birefringence of a phase modulator for circular dichroism by retardation domain analysis. *Opt. Lett.* **2015**, *40*, 1161–1164. [CrossRef] [PubMed]
15. Kewu, L.; Rui, Z.; Ning, J.; Youhua, C.; Minjuan, Z.; Liming, W.; Zhibin, W. Fast and full range measurements of ellipsometric parameters using a 45° dual-drive symmetric photoelastic modulator. *Opt. Express* **2017**, *25*, 5725–5733. [CrossRef] [PubMed]
16. Li, K.; Wang, S.; Wang, L.; Yu, H.; Jing, N.; Xue, R.; Wang, Z. Fast and Sensitive Ellipsometry-Based Biosensing. *Sensors* **2017**, *18*, 15. [CrossRef] [PubMed]

Disclaimer/Publisher's Note: The statements, opinions and data contained in all publications are solely those of the individual author(s) and contributor(s) and not of MDPI and/or the editor(s). MDPI and/or the editor(s) disclaim responsibility for any injury to people or property resulting from any ideas, methods, instructions or products referred to in the content.